Synthesis, engineering, and theory of 2D van der Waals magnets (EP)

(iD) M. Blei, (iD) J. L. Lado, Q. Song, D. Dey, O. Erten, (iD) V. Pardo, R. Comin, S. Tongay, and (iD) A. S. Botana

COLLECTIONS

(EP) This paper was selected as an Editor's Pick

View Online   Export Citation   CrossMark

Synthesis, engineering, and theory of 2D van der Waals magnets EP

M. Blei,[1] J. L. Lado,[2] Q. Song,[3] D. Dey,[4] O. Erten,[4] V. Pardo,[5,6] R. Comin,[3] S. Tongay,[1] and A. S. Botana[4,a]

AFFILIATIONS

[1]Materials Science and Engineering, School for Engineering of Matter, Transport and Energy, Arizona State University, Tempe, Arizona 85287, USA
[2]Department of Applied Physics, Aalto University, Aalto, 00076 Espoo, Finland
[3]Department of Physics, Massachusetts Institute of Technology, Cambridge, Massachusetts 02139, USA
[4]Department of Physics, Arizona State University, Tempe, Arizona 85287, USA
[5]Departamento de Fisica Aplicada, Universidade de Santiago de Compostela, E-15782 Campus Sur s/n, 15704 Santiago de Compostela, Spain
[6]Instituto de Investigacions Tecnoloxicas, Universidade de Santiago de Compostela, E-15782 Campus Sur s/n, 15704 Santiago de Compostela, Spain

[a]Author to whom correspondence should be addressed: antia.botana@asu.edu

ABSTRACT

The recent discovery of magnetism in monolayers of two-dimensional van der Waals materials has opened new venues in materials science and condensed matter physics. Until recently, two-dimensional magnetism remained elusive: Spontaneous magnetic order is a routine instance in three-dimensional materials but it is not *a priori* guaranteed in the two-dimensional world. Since the 2016 discovery of antiferromagnetism in monolayer $FePS_3$ by two groups and the subsequent demonstration of ferromagnetic order in monolayer CrI_3 and bilayer $Cr_2Ge_2Te_6$, the field changed dramatically. Within several years of scientific discoveries focused on 2D magnets, novel opportunities have opened up in the field of spintronics, namely spin pumping devices, spin transfer torque, and tunneling. In this review, we describe the state of the art of the nascent field of magnetic two-dimensional materials focusing on synthesis, engineering, and theory aspects. We also discuss challenges and some of the many different promising directions for future work, highlighting unique applications that may extend even to other realms, including sensing and data storage.

Published under license by AIP Publishing. https://doi.org/10.1063/5.0025658

TABLE OF CONTENTS

I. INTRODUCTION

The recent discovery of magnetism in monolayers of two-dimensional (2D) van der Waals (vdW) materials has opened new venues in materials science and condensed matter physics. Until recently, 2D magnetism remained elusive since the existence of magnetic order in 2D is *a priori* not guaranteed. The story changed in 2016 when two groups provided evidence of antiferromagnetism (AFM) in monolayers of $FePS_3$.[1,2] In 2017, the presence of ferromagnetic (FM) order was proven in monolayers of CrI_3 and on a bilayer of $Cr_2Ge_2Te_6$.[3,4] The list of candidates has been growing ever since.[5–7]

There are various aspects that make 2D vdW crystals with magnetic order very interesting. First, magnetic order in 2D can only happen if there is no continuous rotational symmetry; otherwise, the proliferation of low-energy spin waves, which lie behind the Mermin-Wagner theorem,[8] destroys magnetic order at any finite temperature. Therefore, magnetic anisotropy and spin waves control the transition temperature of 2D magnets and play a much more important role than in their 3D counterparts. Second, the electronic and mechanical properties of 2D materials can be widely tuned in various ways—by gating, proximity, and chemical functionalization—which permit conception of devices where magnetic order is controlled at will. Third, magnetic order adds a new functionality to the set of Lego-like pieces that enriches the game of vertical integration of 2D materials in van der Waals heterostructures. The stacking of materials with magnetic order, superconducting order, spin-valley coupling, and graphene will probably result in structures with completely new and unexpected properties that we can now explore both theoretically and experimentally.

Within just 3 years, the discovery of 2D magnets has already opened up new opportunities in spintronics (i.e., spin pumping devices, spin transfer torque, and tunneling magnetoresistance).[9–11] We envision future applications that may extend into other realms, including sensing and data storage. Here, we review some of the experiments in which magnetism in strictly 2D has been confirmed. We discuss common synthesis techniques for these materials and methods for engineering their magnetic properties. Further, we analyze in detail some of the most important theoretical aspects that need to be considered to understand 2D magnets. Finally, we identify different phenomena that we anticipate will be the next steps to follow in the field.

II. EXPERIMENTAL FINDINGS ON 2D MAGNETS TO DATE
A. Evidence of magnetic order in 2D

We first review some of the existing experiments providing evidence for magnetic order at the monolayer level (or close to it)

and describe briefly the corresponding 2D vdW materials (see Table I).

1. Antiferromagnetism in FePS₃

The first experimental evidence of magnetic order at finite temperature in monolayers was found in $FePS_3$ in 2016. By monitoring the Raman peaks that arise from zone folding due to antiferromagnetic ordering [Fig. 1(a)], it was demonstrated that $FePS_3$ exhibits antiferromagnetic ordering down to the monolayer limit with a Néel temperature (T_N) as high as 118 K.[1,2]

2. Ferromagnetism in CrI₃

Kerr microscopy experiments have shown that ferromagnetism in this material persists down to the monolayer level [Fig. 1(b)] with a large critical temperature of 45 K (not far from that of the bulk $\sim$61 K).[3] Magnetic order in this compound shows an out-of-plane easy-axis anisotropy. The bilayer system [Fig. 1(c)] showed a surprising lack of Kerr signal attributed to an interlayer antiferromagnetic arrangement genuine of the bilayer. Ever since, there has been intense interest in trying to elucidate the importance of stacking order for the magnetic response of this material.[12–15]

3. Antiferromagnetism in CrCl₃

Tunneling magnetoresistance measurements in few-layer $CrCl_3$ provided early evidence of antiferromagnetic ordering down to bilayer samples, as shown in Fig. 1(d).[16] Few-layer samples preserved the same magnetic ordering as their bulk counterparts, with in-plane easy-axis anisotropy, and antiparallel spin–ordering between layers. Strikingly, ultrathin $CrCl_3$ samples showed a 10-fold increase in exchange energy, which was attributed to the different stacking order and its feedback on the out-of-plane exchange interactions at low temperatures. The magnetic phase diagram of $CrCl_3$ multilayers has been established,[17] and recently, it has been suggested that $CrCl_3$ monolayers exhibit ferromagnetic ordering.[18]

4. Ferromagnetism in Cr₂Ge₂Te₆

Magnetic order at the bilayer level was probed in $Cr_2Ge_2Te_6$ by means of Kerr rotation experiments.[4] The monolayer, in turn, was

TABLE I. vdW material systems for which long-range magnetic order has been confirmed experimentally in 2D and their characteristics. AFM, antiferromagnetic; FM, ferromagnetic.

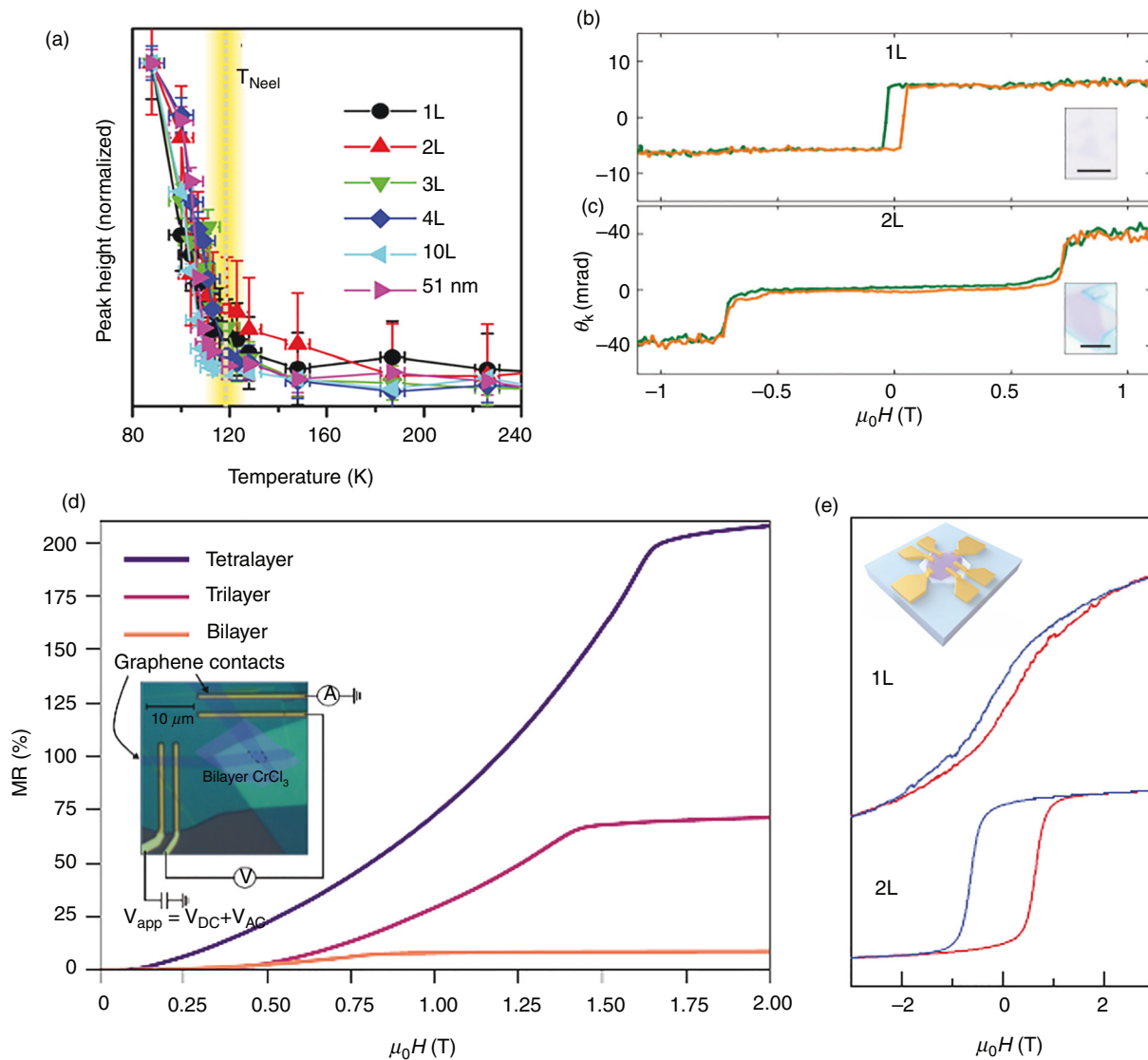| Material	Magnetic order	T_c	Magnetic lattice	Refs.
$FePS_3$	AFM	Zig-zag	Honeycomb	1, 2
CrI_3	FM	45 K	Honeycomb	3,12–15
$CrCl_3$	FM	14 K	Honeycomb	16–18
$Cr_2Ge_2Te_6$	FM	45 K	Honeycomb	4
Fe_3GeTe_2	FM	300 K	Triangular	20, 21
VSe_2	FM	300 K	Triangular	22–26
$MnSe_2$	FM	300 K	Triangular	27

FIG. 1. Characterization of magnetism in 2D. (a) Temperature dependence of the characteristic Raman peak resulting from spin–order-induced folding of the Brillouin zone in FePS$_3$ as a function of thickness. By monitoring the Raman peaks that arise from zone folding due to antiferromagnetic ordering, researchers have demonstrated that FePS$_3$ exhibits antiferromagnetic ordering down to the monolayer limit. Reproduced with permission from Lee *et al.*, Nano Lett. **16**(12), 7433–7438 (2016).[2] Copyright 2016 American Chemical Society. (b) and (c) Magneto-optical Kerr rotation as a function of applied magnetic field in flakes of CrI$_3$, revealing a ferromagnetic (antiferromagnetic) ground state in monolayer (bilayer) samples. The insets show optical microscope images of CrI$_3$ (scale bars = 5 μm). Reproduced with permission from Huang *et al.* Nature **546**(7657), 270–273 (2017). Copyright 2017 Macmillan Publishers Limited, part of Springer Nature.[3] (d) Magnetoresistance (MR) vs applied field in bilayer, trilayer, and tetralayer tunnel junctions of CrCl$_3$ for which antiferromagnetic ordering has been probed down to bilayer samples. Reproduced with permission from Klein *et al.*, Nat. Phys. **15**(12), 1255–1260 (2019). Copyright 2019 Macmillan Publishers Limited, part of Springer Nature.[16] (e) Magnetism was studied in Fe$_3$GeTe$_2$ by probing the Hall resistance. The ferromagnetic transition temperature is suppressed relative to the bulk (205 K), but an ionic gate can raise T$_c$ all the way up to room temperature. Reproduced with permission from Deng *et al.*, Nature **563**, 94–99 (2018). Copyright 2018 Macmillan Publishers Limited, part of Springer Nature.[20]

found to degrade rapidly. The magnetic transition temperature proved to be tunable by means of an external magnetic field that clearly shows the potential to build devices based on 2D vdW magnets with properties that can be easily manipulated. Theoretical studies have analyzed the dependence of the electronic structure and magnetic properties with the number of layers.[19]

5. Ferromagnetism in Fe$_3$GeTe$_2$ (FGT)

Itinerant ferromagnetism persists in Fe$_3$GeTe$_2$ down to the monolayer limit with a sizable out-of-plane magnetocrystalline anisotropy.[20] Magnetism was studied by probing the Hall resistance, as shown in Fig. 1(e). The ferromagnetic transition temperature is

suppressed relative to the bulk (205 K), but an ionic gate can raise T_c all the way up to room temperature, opening up opportunities for potential voltage-controlled magnetoelectronics.[21]

6. Ferromagnetism in transition metal dichalcogenides (TMDs)

A strong ferromagnetic signal at room temperature has been reported at the single-layer level in VSe_2.[22] However, spontaneous ferromagnetism in this system remains a controversial issue due to the possibility of charge density wave (CDW) formation and the subsequent suppression of magnetic order.[22,23] Angle-resolved photoemission spectroscopy (ARPES) and scanning tunneling microscopy (STM) have revealed an electronic reconstruction of single-layer VSe_2 without a detectable FM exchange splitting, casting doubts on whether magnetism originates from an induced band structure spin splitting or whether extrinsic defects come into play.[24–26] Room temperature ferromagnetism has also been reported in $MnSe_2$ films grown by molecular beam epitaxy (MBE). From superconducting quantum interference device (SQUID) measurements in the monolayer limit, the magnetic signal is assigned to intrinsic ferromagnetism with a T_c close to room temperature.[27]

Obviously, other 2D materials are waiting to join this list. In this context, we note that high-throughput computational exfoliation of known 2D vdW materials has been explored targeting the Inorganic Crystal Structure Database. This search identified 56 ferromagnetic and antiferromagnetic candidate systems by analyzing a subset of 258 candidates.[28] Among others, this list includes transition metal dihalides MX_2 and oxyhalides MOX (M = transition metal, X = Cl, Br, I).

B. Common techniques for the synthesis of van der Waals magnetic crystals

After discussing the early magnetic measurements and observations done on 2D magnetic crystals, we focus on common synthesis techniques used for producing layered vdW magnetic crystals. At the time of writing this article, there are no studies that enable researchers to produce monolayer- or few-layer–thick magnetic crystals at large scales using commercially compatible chemical vapor deposition (CVD) or atomic layer deposition (ALD) methods. This is mainly because of the limited environmental stability of some of these 2D magnetic crystals and/or the lack of established surface chemistry routes to enable layer-by-layer deposition.

Because of these limitations, the community currently heavily relies on the production of high-crystalline-quality, defect-free crystals that are ideally free of magnetic impurities such as Fe, Co, and Ni. Once these layered crystals are produced, a routine mechanical exfoliation[29] technique is used to isolate monolayer- to few-layer-thick sheets onto the desired substrates. Depending on the crystal type (halide vs chalcogen based) as well as on their phase diagrams, different crystal growth techniques are used to produce these materials. Based on the most common studies of vdW magnetic crystals in the field, the popular growth techniques include chemical vapor transport (CVT), sublimation, or flux zone techniques, but recent literature has begun to address the challenges outlined at the beginning of this section, and new reports show successful bottom-up synthesis routes for isolating several-layer and monolayer vdW magnets.

1. Chemical vapor transport

Chemical vapor transport is an extremely effective and reliable synthesis technique that can produce macroscale single crystals of layered materials, including the vdW magnetic crystals discussed in Sec. I A.[30–32] In a typical vapor transport experiment, precursor materials are vacuum sealed inside thick-walled quartz ampoules. Due to the high temperatures necessary for growth, in addition to lowering the overall pressure inside the ampoule, vacuum sealing reduces unwanted impurities that may impact the properties of the desired product. The vapor transport direction is governed by Le Chatlier's principle, where precursor materials are transported from a source to a sink, meaning that endothermic reactions transport from a hot zone to a cold zone and exothermic reactions transport from a cold zone to a hot zone. A suitable transport agent must also be chosen to ensure that the precursors achieve a gaseous state, which is a prerequisite for vapor transport to occur, as discussed in great length by Binnewies *et al.*[33,34] For example, transition metal thiophosphate crystal synthesis (e.g., $MnPS_3$, $FePS_3$, and $CoPS_3$) typically involves the use of halides (I_2, Br_2, etc.) as transport agents to produce these vdW crystals.[30] Since CrI_3 crystals already contain iodine in the crystal matrix, the reaction of elemental Cr and I_2 in a quartz ampoule is sufficient.[35]

2. Sublimation

In addition to CVT, physical vapor transport (PVT), or sublimation, is another method that can be used to produce high-quality single crystals of transition metal halides.[36,37] It has proven to be a useful and low-cost technique that does not require sophisticated ampoule sealing processes necessary for chemical vapor transport reactions, although evacuated and sealed ampoules may also be used to carry out the growth.[38] For the synthesis of $CrCl_3$ and other transition metal halides, commercially available compounds are placed in an open-ended or sealed quartz tube and positioned in a horizontal furnace with the desired temperature gradient. No additional transport agent is required as these materials contain the necessary halide and self-transport. After heating the compound to its respective sublimation point, the transition metal halides transport to the cold zone of the furnace where they nucleate and grow directly on the walls of the quartz tube. Large, high-quality crystals can be obtained in 24–48 h.[39]

3. Flux zone growth

While the previously discussed vapor phase synthesis techniques can be used for transition metal halides, other classes of 2D vdW magnets, such as $Cr_2Ge_2Te_3$ and Fe_3GeTe_2, can be obtained from solution-phase flux methods to achieve large, high-quality crystals.[40–42] For this method, stoichiometric amounts of precursors and flux (solvent) are loaded into an inert crucible, such as quartz, and vacuum sealed ($\sim 10^{-5}$ Torr). Because the precursors and flux are in direct contact with the crucible, careful selection of the crucible material must be made to ensure that no undesirable reactions occur between the crucible and the precursors. Additionally, the inorganic flux is chosen, among other factors, to have a high solubility of the desired elements at the growth temperature, not to create any competing phases, and in many cases, a self-flux can be part of the chemical composition of the resultant product. In the case of $Cr_2Ge_2Te_6$, excess germanium and tellurium are used to create a self-flux. The precursors and flux are then

heated above their melting temperatures and slowly cooled over a period of several days. As the solution slowly cools, the desired materials precipitate out of the flux, where they spontaneously nucleate and crystalize. Growth parameters are selected based on prior knowledge of the product's binary or ternary phase diagrams, but experimentally, determining and optimizing the growth parameters are often necessary because phase diagrams have not been fully established for the desired material system. After the growth is complete, the final step is to remove the flux from the crystal. The most common method to remove the flux from tellurium-based vdW magnets is to melt the tellurium and remove it through a centrifugation process, and depending on the flux, additional steps may be required to fully remove the flux.[43]

4. Advancements in thin-film synthesis

While the crystal growth techniques discussed in Sec. II B are well-established methods and have proven useful for the discovery of 2D vdW magnets, they have limited applications for the industrial manufacturing of electronic devices. Isolating few-layers and monolayers of materials grown by bulk synthesis methods require top-down approaches to deposit them on suitable substrates, the most popular being the well-known Scotch tape technique introduced by Novoselov *et al.*[29] and others.[44–46] This has proven to be an excellent method to study the intrinsic properties of vdW crystals in their low-dimensional limit. However, if the next-generation materials for quantum electronics are to be realized, rapid progress toward the growth of reliable, large-area thin films and monolayers must be made. In this context, studies using CVT to produce thin films of vdW magnets on a variety of substrates have recently been performed.[47–49] Rather than empirically determining favorable growth conditions, computational modeling of the elemental chemical transport is done first, allowing the simulation of transport reactions for a number of 2D vdW magnetic materials. For the chromium-trihalide family, it was found that $CrBr_3$ and CrI_3 would be best synthesized by traditional CVT, while direct sublimation of $CrCl_3$ would be the best approach. Transport rates determined using this method allow estimates to be obtained of the most favorable growth times and temperatures to deposit these materials without performing exhaustive and expensive empirical studies. X-ray photoelectron spectroscopy (XPS) and other characterization techniques determined the successful synthesis of CrX_3 (X = Cl, Br, I) on yttrium-stabilized zirconia substrates with limited detectable impurities. Results from this work may extend to other material classes and could be used as a test bed to understand nucleation and growth dynamics in a closed system prior to developing highly specific CVD and ALD systems.

MBE has traditionally been used as a tool to epitaxially synthesize low-dimensional materials of all types before they are realized using larger-scale commercial systems. Several vdW magnetic systems are currently being studied and synthesized using MBE.[50,51] While we cannot discuss every synthesis article surrounding this topic, highlighting recent developments toward mono- or few-layer growth of material systems is important. In 2019, the first report of MBE-grown $CrBr_3$ was published,[52] and most recently, a comprehensive study of CrI_3 and CrI_2 synthesized by MBE was performed.[53] This latter work demonstrates that monolayer Cr-based di- and trihalides can be epitaxially grown on HOPG and Au (111) substrates using a home-built

MBE-STM (scanning tunneling microscope), where CrI_3 powder was used as the source of iodine because of its compatibility with ultra-high vacuum (UHV) chambers. AFM, XPS, and STM revealed that CrI_3 prefers to form multiphase superstructures, creating networks of Moiré patterns on Au (111), and that single-crystal monolayers of CrI_3 could reliably be grown on HOPG. Furthermore, the stoichiometry of CrI_x (x = 2, 3) films could be controlled via different thermal processing routes. These findings give massive insight into producing transition metal halides at larger scales.

5. Vapor deposition

At present, there is very limited research showing successful synthesis of layered magnetic crystals using CVD- or physical vapor deposition (PVD)–based techniques. However, recent reports have expanded the library of vdW materials that may be synthesized by these methods, with the most common systems being chalcogen-based binary and ternary compounds, such as VSe_2 and $NiPS_3$, among others.[50,54–58] However, new insights may be derived from recent work, where for the first time, pnictogen and halogen-based vdW magnets have been synthesized via chemical and physical vapor deposition routes.[59,60] In 2020, the first growth of NiI_2 synthesized by PVD was reported.[60] This is a massive feat due to the difficulty of controlling the gaseous species inside the reaction chamber, as high vapor pressures and low sublimation points of precursors present numerous challenges to growth dynamics. NiI_2 was epitaxially grown on hexagonal boron nitride (hBN) and Si/SiO_2 using a conventional single-zone tube furnace at ambient pressure and relatively low temperatures ($\sim$450 °C) with NiI_2 powder and Ar gas as a carrier. Prior to deposition, commercially sourced hBN was mechanically exfoliated and transferred onto $Si/SiO2$ substrates and calcined to eliminate any unwanted impurities. Raman spectroscopy, energy dispersive spectroscopy (EDS), XPS, and atomic force microscopy confirmed the successful synthesis of mono- and few-layer NiI_2 on hBN and thicker films of NiI_2 on bare Si/SiO_2 substrates not covered by hBN.

C. Engineering magnetism in 2D

A significant advantage of 2D materials is that their physical properties are highly tunable by means of external control parameters that include electrostatic doping, pressure, and strain. Here, we highlight a few recent demonstrations of tunable magnetism in 2D materials.

1. Electrostatic doping

Electrostatic doping is a powerful technique for tuning the electronic properties of 2D materials. The working principle is similar to that underlying field-effect transistors and is based on the direct transfer of electronic or ionic charges from a dielectric into the target 2D material. Electrostatic doping has a series of advantages over chemical doping of bulk materials. It is continuously controllable through a gate bias, it is compatible with a variety of dopant species from simple electrons/holes to specific ions/chemical functional groups, and it can be applied to most 2D materials without being hindered by phase separation issues in nonstoichiometric bulk synthesis. It has been shown that the electrostatic doping in 2D materials could unveil new physics, such

as unconventional superconductivity in MoS_2,[61] twisted bilayer graphene,[62] or structural transitions in $MoTe_2$.[63]

As mentioned in Sec. II A 3, bilayer CrI_3 is a layered antiferromagnet, and it was found that the interlayer exchange coupling is tunable by electrostatic doping. Figure 2(a) shows the schematic of the representative bilayer CrI_3 device. This device is a vertical stack of a bilayer CrI_3 flake and a graphite contact encapsulated between two hBN flakes and a graphite top gate. By applying the gate voltage to the insulator hBN, the electric dipoles at the hBN-CrI_3 interface introduce carrier injection into the bilayer CrI_3. Figure 2(b) shows the reflection magnetic circular dichroism (RMCD) signal as a function of both top- and back-gate voltages near the metamagnetic transition field $\mu_0H = 0.78$ T. The red region on the right is the signal from the $\uparrow\uparrow$ state, and the pink region on the left is from the layered AFM state. The dashed line boundary indicates that the metamagnetic transition could be effectively tuned by electrostatic doping.[64,65]

FGT is a layered ferromagnet with bulk $T_c = 205$ K. In monolayer FGT, however, the ferromagnetic transition temperature is suppressed due to thermal fluctuations of long-wavelength acoustic-like magnon modes in 2D, while the trilayer sample has a T_c of $\sim$100 K. Strikingly, ionic liquid gating could raise T_c to room temperature, much higher than the bulk T_c [Fig. 2(d)]. This ionic gating method [Fig. 2(c)] intercalates the Li^+ from $LiClO_4$ (the transparent liquid electrolyte) onto the surface of the FGT by the gate voltage V_g, and the doping level could reach values as high as 10^{14} cm^{-2}, which is one order of magnitude higher than those achievable using hBN gates.[20]

2. Pressure

In a vdW material, a small change of the interlayer spacing can cause a drastic change in physical properties. In particular, if the material supports magnetism, the interlayer interactions can be modified to produce a change in the magnitude and sign of the exchange coupling.
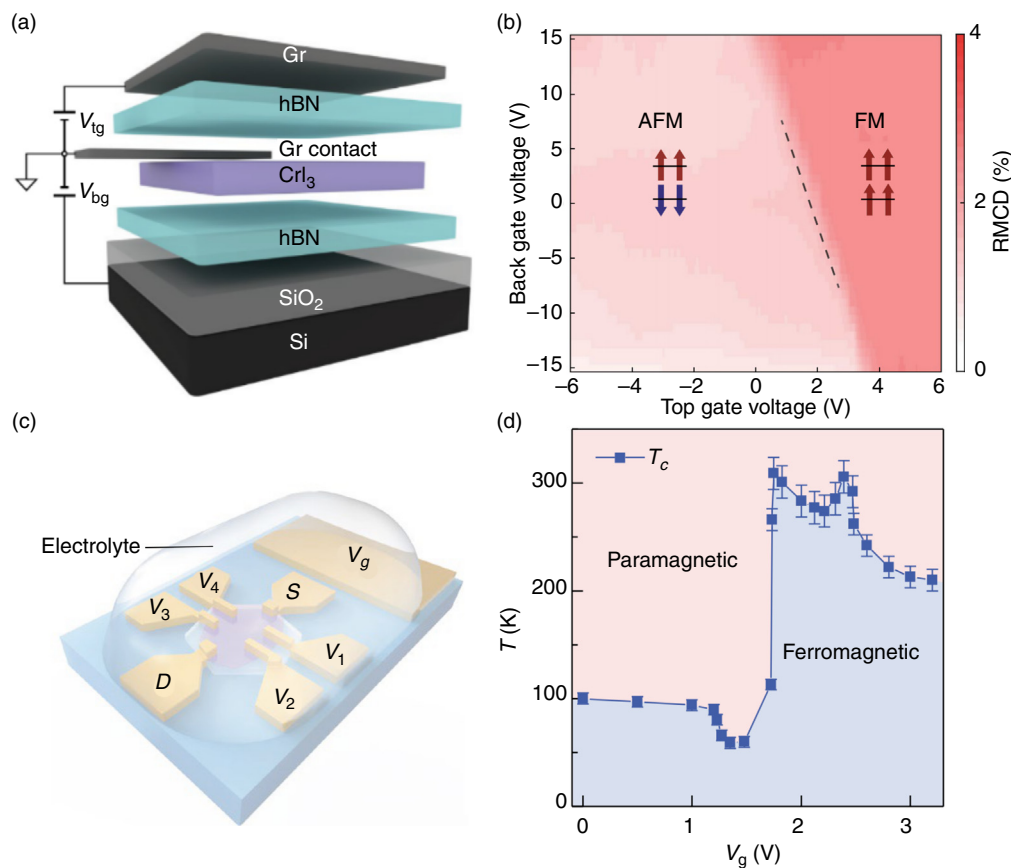

FIG. 2. Gate-tunable magnetism of CrI_3 and FGT. (a) Schematic of a dual-gated bilayer CrI_3 device. The device is a vertical stack of a bilayer CrI_3 flake and a graphite contact encapsulated between two hBN flakes and a graphite top gate. By applying the gate voltage to the insulator hBN, the electric dipoles at the hBN-CrI_3 interface introduce carrier injection into the bilayer CrI_3. (b) RMCD signal of the electrostatic doped bilayer CrI_3. The dashed contour shows the tunable metamagnetic transition field through bias voltage. Reproduced with permission from Huang et al., Nat. Nanotech. **13**(7), 544–548 (2018). Copyright 2018 Macmillan Publishers Limited, part of Springer Nature.[65] (c) Schematic of the FGT device structure and measurement setup. S and D label the source and drain electrodes, respectively, and V_1, V_2, V_3, and V_4 label the voltage probes. The solid electrolyte ($LiClO_4$ dissolved in polyethylene oxide matrix) covers both the FGT flake and the side gate. (d) Phase diagram of the trilayer FGT sample as the gate voltage and temperature are varied. The transition temperature is determined from the extrapolation of the temperature-dependent anomalous Hall resistance to zero. Reproduced with permission from Deng et al., Nature **563**, 94–99 (2018). Copyright 2018 Macmillan Publishers Limited, part of Springer Nature.[20]
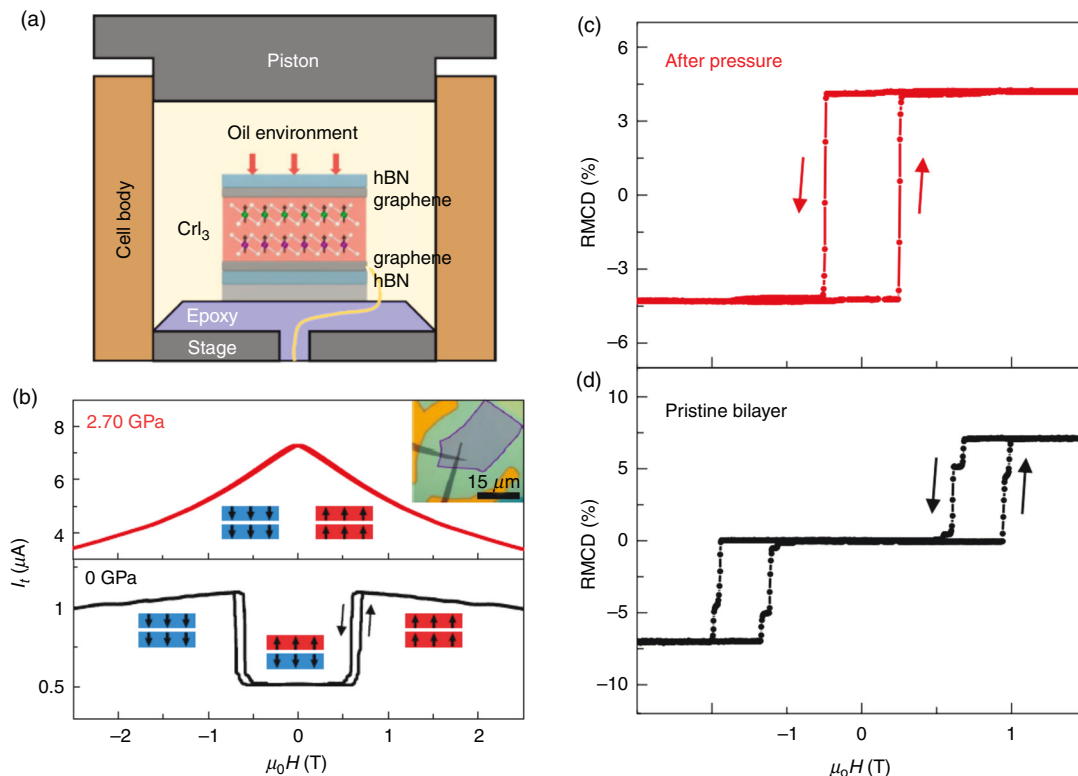
FIG. 3. High-pressure study of CrI₃. (a) Schematic of a high-pressure experimental setup. Here, a magnetic tunnel junction device is composed of bilayer CrI₃ sandwiched between top and bottom multilayer graphene contacts. The entire MTJ was encapsulated by hBN to prevent sample degradation. The device was then held in a piston cylinder cell filled with oil for application of hydrostatic pressure. The force applied to the piston exerts pressure on the bilayer CrI₃ device through oil. (b) Magnetic states are probed by using tunneling current vs magnetic field H. Measurements at two different pressures are shown. Insets show magnetic states and an optical microscopy image of a bilayer device. (c) and (d) As demonstrated in Ref. 68, after removal from the cell, reflective magnetic circular dichroism microscopy highlighted that the bilayer CrI₃ irreversibly transitioned from antiferromagnetic to ferromagnetic ordering. Reproduced with permission from Song *et al.*, Nat. Mater. **18**(12), 1298–1302 (2019). Copyright 2019 Macmillan Publishers Limited, part of Springer Nature.[68]

Hydrostatic pressure is a typical method for continuous control of interlayer coupling via interlayer spacing in vdW crystals.[66]

Figure 3(a) shows a schematic of the experimental setup of a high-pressure study of CrI₃. A magnetic tunnel junction (MTJ) device was composed of bilayer CrI₃ sandwiched between top and bottom multilayer graphene contacts. The entire MTJ was encapsulated by hBN to prevent sample degradation. The device was then held in a piston cylinder cell filled with oil for application of hydrostatic pressure. Magnetic states were probed by using tunneling magnetoresistance measurements as shown in Fig. 3(b). After removal from the cell, RMCD microscopy [Fig. 3(c) and 3(d)] showed that the bilayer CrI₃ irreversibly transitioned from antiferromagnetic to ferromagnetic ordering.[67,68]

3. Strain

2D materials possess outstanding mechanical properties and can sustain larger strain than their bulk counterparts. Monolayer MoS₂ is predicted to sustain elastic strain levels up to 11% and monolayer FeSe up to 6%.[69,70] Strain engineering has been shown to be an effective approach to tune the properties of 2D materials using various methods, including substrate-lattice mismatch,[71,72] mechanically actuated strain cells,[73,74] and nanomechanical drumheads.[75]

Figure 4(a) shows the experimental setup used in the biaxial strain study of bilayer CrI₃ through the nanomechanical drumhead. By applying a voltage to the silicon substrate, the electrostatic force between silicon and CrI₃ can apply tensile biaxial strain to CrI₃ itself. Figure 4(b) shows the structure of the bilayer CrI₃ device, with CrI₃ encapsulated within two stable 2D materials: few-layer graphene at the bottom and monolayer WSe₂ on top. In addition to protecting CrI₃ from degradation under ambient conditions, few-layer graphene acts as a conducting electrode, while monolayer WSe₂ provides a strain gauge via measurements of the shift in the exciton energy (under the assumption that WSe₂ experiences the same level of strain as CrI₃). This 2D heterostructure was first assembled and then transferred on prefabricated circular microtrenches with patterned Au electrodes and Si back gate [Fig. 4(c)]. Figure 4(d) shows that the metamagnetic transition field in bilayer CrI₃ could be tuned effectively by applying tensile biaxial strain.[75]

III. THEORY OF MAGNETISM IN 2D
A. Background

Symmetry breaking in low-dimensional systems plays a very special role in condensed matter physics. The spontaneous breaking of a continuous symmetry is not possible in two dimensions at finite temperature unless long-range interactions come into play. Analogous
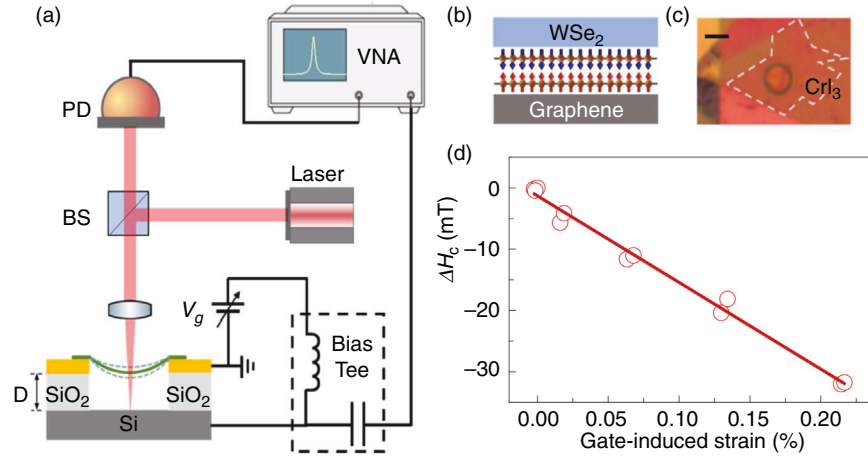
FIG. 4. Biaxial strain study of CrI$_3$. (a) Schematic of the measurement system. A DC voltage V$_g$ is imposed to apply electrostatic force to the membrane. The laser is used to detect both the strain and magnetic ordering. BS, beam splitter; PD, photodetector. (b) Schematic of a bilayer CrI$_3$ device, with CrI$_3$ encapsulated within two stable 2D materials: few-layer graphene at the bottom and monolayer WSe$_2$ on top. Apart from protecting CrI$_3$ from degradation under ambient conditions, the few-layer graphene acts as a conducting electrode, while monolayer WSe$_2$ provides a strain gauge via measurements of the shift in the exciton energy. (c) Optical microscope image of a bilayer CrI$_3$ device. The aforementioned 2D heterostructure was first assembled and then transferred on prefabricated circular microtrenches with patterned Au electrodes and Si back gate. (d) The metamagnetic transition field as a function of gate-induced strain (circles); the solid line is a linear fit. Reproduced with permission from Jiang *et al.*, Nat. Mater. **19**, 1295–1299 (2020). Copyright 2020 Macmillan Publishers Limited, part of Springer Nature.[75]

propositions were posed, in the form of mathematical theorems, in the context of crystalline order by Landau and Peierls, in the context of superconductors and superfluids by Hohenberg,[76] and in the context of magnetism by Mermin and Wagner.[8] The common ground of all these theorems is the existence of gapless collective excitations—the Goldstone modes—each of which is associated with the order parameter of the broken symmetry phase. In the case of magnets, these Goldstone modes are spin waves (or magnons), and in two (and one) dimensions, the thermal population of these low-energy excitations completely destroys long-range order. This is exemplified by computing the correction to the magnetization within spin wave theory for an isotropic ferromagnet that yields a divergent result in two dimensions,

$$\delta M(T) \sim \int_0^\infty \frac{k\,dk}{e^{\beta \rho k^2} - 1} \to \infty, \tag{1}$$

where $\delta M(T)$ refers to the correction to the magnetization due to thermal fluctuations and ρ and β are the spin wave stiffness and inverse temperature.

1. Spin Hamiltonian

A very wide class of magnetic materials are insulating. Therefore, charge degrees of freedom are frozen, and it is possible to describe their magnetic properties in terms of spin Hamiltonians (even in the case of conducting magnetic materials, their magnetic properties can also be described fairly well with effective spin Hamiltonians). So, it is adequate to start our discussion with a brief description of a simplified spin Hamiltonian,

$$H = -\sum_{\langle ij \rangle} J_{ij}\,\mathbf{S}_i \cdot \mathbf{S}_j - \sum_{\langle ij \rangle} K_{ij} S_i^z S_j^z - \sum_i D_i \left(S_i^z\right)^2 + \sum_i \mathbf{B} \cdot \mathbf{S}_i. \tag{2}$$

The first term describes the exchange (Heisenberg) interactions, the second the anisotropic exchange, and the third the single-ion

anisotropy; the fourth introduces the effect of an external magnetic field. We note that additional anisotropic terms could be allowed, such as Kitaev,[77] biquadratic exchange,[78] or Dzyaloshinsky-Moriya[79] interactions (DMI).

The divergent result of Eq. 1 could be avoided if the spin wave spectra have a gap (mechanism 1) or the dispersion of the spin wave is different (mechanism 2). Mechanism 1 corresponds to the existence of a single-ion anisotropy or anisotropic exchange, which yields ferromagnetism in CrI$_3$[3] and Fe$_3$GeTe$_2$.[21] Mechanism 2 corresponds to the correction to the spin wave dispersion due to dipolar interactions. Dipolar interactions could allow stabilization of in-plane ferromagnetic order, yet such a scenario has not been confirmed in a 2D van der Waals material to date. With the previous dispersion relation, the correction to the magnetization within the linear spin wave regime becomes at low temperatures $k_B T \ll \Delta$, which yields a finite correction to the maximal magnetization at low enough temperatures, thus allowing for a ferromagnetic state at finite temperatures,

$$\delta M(T) \sim \int_0^\infty \frac{k\,dk}{e^{\beta(\Delta + \rho k^2)} - 1} \to \frac{1}{\beta}\,e^{-\beta\Delta}. \tag{3}$$

B. Origin of magnetic anisotropies

1. Single-ion anisotropy

The simplest anisotropic term that can be written is the so-called uniaxial single-ion anisotropy, which takes the form:

$$H_{SIA} = -D \sum_i \left(S_i^z\right)^2. \tag{4}$$

The parameter D favors off-plane magnetism for $D > 0$, whereas it favors in-plane magnetism for $D < 0$. For $D \gg J$, the Heisenberg model reduces to the Ising model. It must be noted that for $S = 1/2$, $S^2 = 1/4$,

and thus, the previous term is trivial, yielding that $S = 1/2$ ferromagnets cannot have single-ion anisotropy.

The physical origin of this term is the interplay between the local crystal field δ and the atomic spin–orbit coupling λ. Such anisotropic terms in the Hamiltonian stem from perturbation theory in the high-spin state of the ion and crucially depend on the spin–orbit coupling of the magnetic ion. We can distinguish between two different cases: systems with orbital degeneracy and systems without orbital degeneracy. In systems with orbital degeneracy, the single-ion anisotropy is first order in λ, yet orbital degeneracy can be easily lifted by a Jahn–Teller mechanism. In the absence of orbital degeneracy, the single-ion anisotropy stems (at least) from second-order perturbation in λ/δ, yielding $D \sim (\lambda/\delta)^2$.

Single-ion anisotropy is expected to be strong for transition metals whose crystal field environment has a well-defined symmetry axis as in the 2H transition metal dichalcogenide structure. In contrast, for approximate octahedral environments, such as those in 1T-TMDs or in CrI_3, the magnitude of the trigonal distortion is expected to substantially impact the value of the single-ion anisotropy D.

2. Exchange anisotropy

The second source of a gap in the spin wave Hamiltonian is the anisotropic exchange that takes the form,

$$H_{AI} = -K \sum_{\langle ij \rangle} S_i^z S_j^z, \tag{5}$$

where ij denotes sum over first neighbors. For a ferromagnet, the previous term favors a parallel off-plane alignment for $K > 0$, whereas for $K < 0$, in-plane magnetism is favored. We note that this term yields a nontrivial contribution for an $S = 1/2$ system and, thus, can yield a magnon gap for an $S = 1/2$ ferromagnet.

Physically, the origin of the anisotropic exchange K stems from the connecting atoms between two localized spins. Importantly, in this situation, K is mainly controlled by the spin–orbit coupling of the bonding atom instead of the magnetic one. A particular example of this is CrI_3, where the anisotropy energy is controlled by the strength of the spin–orbit coupling of iodine. Generically, 2D magnets with heavy anions, such as Br, I, and Te, are susceptible to have sizable contributions to the anisotropic exchange due to the large spin–orbit coupling of the ligand anion.[80] The relative strength of the single-ion anisotropy and anisotropic exchange can be estimated from first principles methods, yet their exact values can be sensitive to the details of the method.[80,81]

If the dominant correlations in a honeycomb lattice of $S = 1/2$ ions are AFM, then the presence of strong spin–orbit coupling may lead to anisotropic exchange couplings and satisfy the requirements for a Kitaev model[82] to be applicable. A prominent example of this is $RuCl_3$.[83] We describe this material in more detail in Sec. IV C in the context of platforms for quantum spin-liquid (QSL) realization.

3. Dipolar anisotropy

Dipolar interactions represent an additional mechanism to stabilize magnetic ordering in 2D. In particular, they may allow stabilization of in-plane magnetic ordering at a finite temperature. Dipolar interactions favor an in-plane arrangement of spins, yielding a

Hamiltonian with in-plane rotational symmetry. This leads to the so-called reorientation transition observed in ferromagnetic thin films that stems from the thermal renormalization of the anisotropy.[84] Moreover, dipolar interactions modify the spin wave spectra so that at low energies, the magnon dispersion becomes $E_k \propto k^{1/2}$, yielding the integral in Eq. 1 nondivergent. However, van der Waals ferromagnets with in-plane anisotropy are highly elusive, and assessing the existence of in-plane ferromagnetic ordering in van der Waals systems remains an open question.

C. Heisenberg Hamiltonian: Origin of magnetic exchanges

The strengths and signs of the exchange couplings between different atoms depend on microscopic details and often arise from a complex interplay between hopping and electronic interactions. Nevertheless, for those cases in the localized limit (i.e., with the active electrons being strongly localized in the magnetic ions), the signs of the different exchange interactions can be predicted using the well-known Goodenough-Kanamori rules.[85]

Most of the existing two-dimensional systems that have shown magnetic long-range order in the single-layer limit present structures with some common motifs: hexagonal or triangular lattices in the plane (see Table I) and cations in an octahedral environment of their neighboring anions, with these octahedra being connected via edge sharing. Most of these systems, such as transition metal dihalides and trihalides,[86,87] transition metal dichalcogenides crystallizing in the 1T structure,[88] $Cr_2Ge_2Te_6$,[89] and compounds of the AMX_3 type[90] (including phosphosulphides and phosphoselenides), can be interpreted in the localized electron limit since most of them are magnetic semiconductors both in their bulk and few-layer form. In this situation, it is important to analyze the possible mechanisms for exchange in such structures. There will be an important contribution coming from direct exchange (metal-metal), and another one coming via an anion, where the cation-anion-cation path forms an angle of $\sim 90°$ (superexchange). These structural details can be observed in Fig. 5, which depicts the structure of $FePS_3$,[91] as an example of a case of a hexagonal in-plane network and the close-up case of two neighboring octahedra sharing an edge. We note that transition metal dichalcogenides can crystallize in the 2H structure with a trigonal prismatic environment
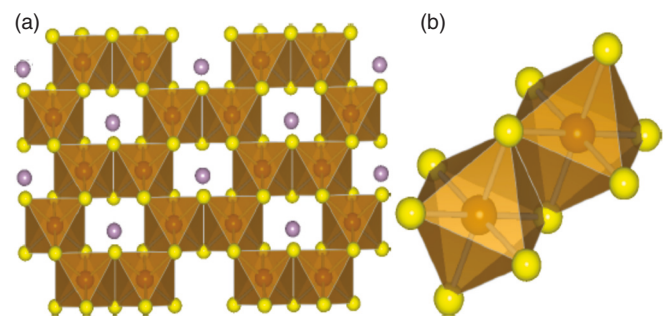

FIG. 5. (a) Structure of $FePS_3$ as seen from the top of the hexagonal plane. (b) Two transition metal atoms surrounded by an ionic octahedral cage. The octahedra are edge sharing. This is the typical coordination in most known 2D vdW magnets. In this situation, competition between metal-metal direct exchange and 90° superexchange via anions can take place as discussed in the text.

around the cations rather than an octahedral one. However, although the important points necessary to understand the magnetic couplings involved for such a case are included in our analysis, the crystal field splittings would be different with respect to the octahedral case.

We now analyze magnetic exchanges for various relevant fillings of the external d shell and discuss how ferromagnetic ordering may emerge. We will use transition metal halides (in which 2D magnetism has been experimentally confirmed or theoretically proposed) as a practical example to discuss the evolution of magnetic interactions with d filling and anion size. The important point to follow the discussion would be that as the anion increases in size (going down in its respective column in the periodic table) it gives rise to a larger cation-cation distance, which decreases the strength of the direct exchange. However, the metal-anion-metal interaction is much less affected by such change. Thus, if both couplings have the same sign, increasing the anion size simply leads to a reduction in the magnetic transition temperature. However, if they have opposite signs, as the anion size increases, the sign of the superexchange becomes more important. Table II compiles all the analyzed d fillings that may lead to FM long-range order. Other fillings (such as d^1, d^4, d^5 low spin, or d^9)[92–95] lead to dominant AFM correlations, and we do not include them here. We will discuss separately the physics of the spin-1/2 honeycomb lattice (d^1 or d^5 low spin) in Sec. IV C. We will also leave aside the complex orbital physics that determines the competition between FM and AFM coupling for d^2 filling, as in VI_3.[96–98]

1. d^3 filling

There is active competition between an AFM direct exchange and a FM superexchange. Direct exchange decreases its strength as a larger anion is introduced, and hence, the cation-cation distance is increased. Hence, the tendency for ferromagnetism is enlarged as the unit cell size increases. In Cr trihalides, it is experimentally observed that the FM Curie temperature increases with anion size (17 K for Cl, 33 K for Br, 68 K for I).[99] In the case of V dihalides, the AFM Néel temperature decreases as the anion size increases (36 K for Cl, 30 K for Br, 16 K for I),[100] indicating a larger importance of the FM component as the cation-cation distance increases.

2. d^5 filling

There is also a competition between AFM direct exchange and FM superexchange. Additionally, there is a competition in the

superexchange between that coming from σ-bonding (mediated by the e_g electrons), which is FM, and that due to π-bonding (t_{2g}-mediated), which is AFM. In the case of high-spin d^5 cations, the FM component becomes important. This competition causes the appearance of a helical phase in $FeCl_3$[101] and a striped phase in Mn dihalides.

3. d^6 filling

In this case, there is no competition; both direct exchange and superexchange yield an FM component. That is why in the Fe dihalides, the Curie temperature[81] is higher for $FeCl_2$ (38 K) than for $FeBr_2$ (14 K); a lower T_c occurs when the cation-cation separation increases.

4. d^7 filling

Again, there is no competition between direct exchange and superexchange, both being FM. An example of this is the Co dihalides. The Curie temperature is reduced when going from $CoCl_2$ to CoI_2[87,102] (11 K for CoI_2, 19 K for $CoBr_2$, and 25 K for $CoCl_2$), as the anion size increases leading to a larger Co-Co distance that decreases the magnetic interaction strength, in particular, the direct component.

5. d^8 filling

In this case, there is competition between an AFM direct exchange and FM superexchange. Ni dihalides exemplify this competition as they are FM in-plane and their Curie temperature increases as the size of the anion does because the AFM component of the total exchange becomes reduced as the cation-cation distance increases (NiI_2 has a Curie temperature of 75 K and that of the smaller anion $NiCl_2$ is 52 K[87]).

IV. OVERALL OUTLOOK
A. Multiferroics

Multiferroics are materials showing a coexisting magnetic and ferroelectric order. Ferroelectric order is the spontaneous development of a finite electric dipole in a material, analogous to the magnetic ordering of a ferromagnet. Ferromagnetism and ferroelectricity are known to obstruct each other. The simplest case is the one of perovskites, where displacive ferroelectricity is favored by an empty d shell, whereas ferromagnetism requires a partially filled d shell. As a result, realizing multiferroic orders requires a nondisplacive mechanism for ferroelectricity, such as charge order, spin-driven, electronic lone pair, or geometric effects. Multiferroic two-dimensional materials would have important applications, including electric reversal of magnetization[103] or electrically controlling an exchange bias.[104] Similar effects have been obtained in two-dimensional heterostructures, as for instance, in CrI_3 bilayers,[63,64] yet without relying on a multiferroic effect. Multiferroicity has been predicted to intrinsically appear in two-dimensional materials, such as transition metal phosphorus chalcogenides,[105] $CuBr_2$,[106,107] and VOI_2.[108] Interestingly, artificial multiferroics can be engineered in ferroelectric/ferromagnetic van der Waals heterostructures.[105]

B. Skyrmions

The interplay of ferromagnetic interactions, DMI, and an external magnetic field can turn a skyrmion configuration energetically

TABLE II. Summary of the magnetic couplings[85] discussed in the text for edge-sharing octahedra at various fillings of the 3D shell, with examples of representative cations. All cases considered are high spin. If the two couplings have opposite signs, competition is active. The table is limited to the fillings where ferromagnetism can become the dominant long-range interaction. AFM, antiferromagnetic; FM, ferromagnetic.

Filling	Cations	Direct exchange	90° superexchange	Competition
d^3	V^{2+}, Cr^{3+}	AFM	FM	Yes
d^5	Mn^{2+}, Fe^{3+}	AFM	FM	Yes
d^6	Fe^{2+}	FM	FM	No
d^7	Co^{2+}	FM	FM	No
d^8	Ni^{2+}	AFM	FM	Yes

TABLE III. Theoretical prediction for magnetic exchanges in Janus materials.

Material	J (meV)	DMI (meV)	K (meV)	Refs.
$Cr(I, Br)_3$	−1.800	0.270	0.505	113
$Cr(I, Cl)_3$	−0.983	0.191	0.422	113
MnSTe	6–10.52	(−0.04)–2.14	0.29	111, 114
MnSeTe	12.9–13.26	5.58–2.63	0.37	111, 114
MnSSe	25.1–15.60	1.25	0.07	111, 114
VSeTe	2.2	4.34	—	114, 115

favorable over the spin-spiral and ferromagnetic states. In addition to their fundamental interest, skyrmions in 2D vdW materials could provide a new paradigm for low-power data storage. At this point, a few theoretical proposals of skyrmion formation in 2D vdW materials exist. These include twisting in vdW heterostructures, in particular using the example of a ferromagnetic monolayer on top of an antiferromagnet.[109,110] An exciting possibility is skyrmion formation via inversion symmetry breaking in transition metal Janus dichalcogenide monolayers that can achieve DMI values comparable to "traditional" skyrmion-hosting materials.[111] Table III shows theoretical predictions for exchange interaction, DMI, and anisotropy values for candidate Janus magnets. Another proposal shows that in CrI_3 monolayers, skyrmion spin configurations become more stable than FM ones by applying an out-of-plane electric field.[112]

Recently, the first experimental observation of magnetic skyrmions in the 2D vdW ferromagnet Fe_3GeTe_2 was reported using high-resolution scanning transmission x-ray microscopy (STXM) and Lorentz transmission electron microscopy measurements [Fig. 6(a)]. A skyrmion crystal state can be generated both dynamically using current pulses and statically using canted magnetic fields[116] [Fig. 6(b)].

C. Quantum spin-liquids

QSLs are a class of quantum-disordered phases where reduced dimensionality, geometric frustration, and quantum fluctuations completely destroy long-range magnetic order down to zero temperature. QSLs are intriguing as they exhibit topological entanglement entropy as well as fractionalized excitations that obey emergent gauge fields (see Ref. 117 for a recent review). Experimental searches for QSLs mostly targeted layered magnets, whereas the majority of the theoretical studies are for two-dimensional models. Therefore, 2D vdW magnets provide a unique opportunity to discover new QSLs. Two promising routes are the (1) honeycomb lattices with Kitaev exchange and (2) triangular lattices with frustrated interactions. Examples of such systems include the aforementioned α-RuCl$_3$,[118–122] KV$_3$Sb$_5$,[123] and Os$_{0.55}$Cl$_2$.[124] Figure 7(a) shows the thermal hall conductivity when applying a tilted magnetic field on α-RuCl$_3$ at different temperatures, and the half-integer plateau indicates the Majorana fermion, a signature of a Kitaev spin-liquid phase. Figure 7(b) shows the phase diagram of α-RuCl$_3$ in a field tilted at $\theta = 60°$ (right inset). Below $T \approx J_K/k_B \approx 80$ K, the spin-liquid (Kitaev paramagnetic) state appears and the half-integer quantized plateau of the 2D thermal Hall conductance is observed in the red area.[120]

D. From the synthesis perspective

While traditional synthesis methods are a logical choice for fundamental research in order to identify the most promising 2D vdW magnets, more comprehensive crystal growth studies are needed to understand how crystal growth techniques, thermal profile, and precursor types ultimately influence the fundamental behavior of vdW magnetic crystals. The current literature heavily relies on a half-a-century-old crystal growth method, and while these techniques are well established to produce these crystals, prior literature has given very little attention to magnetic quantum phenomena in 2D. Thus, more careful crystal growth studies are needed to pinpoint how defect density can be reduced, how crystalline quality can be improved, and how magnetic impurities can be eliminated. Clearly, new crystal growth techniques or recipes will be required to produce recently predicted 2D vdW magnets. This is a challenging task, especially for ternary and quaternary systems wherein many different phases or compositions
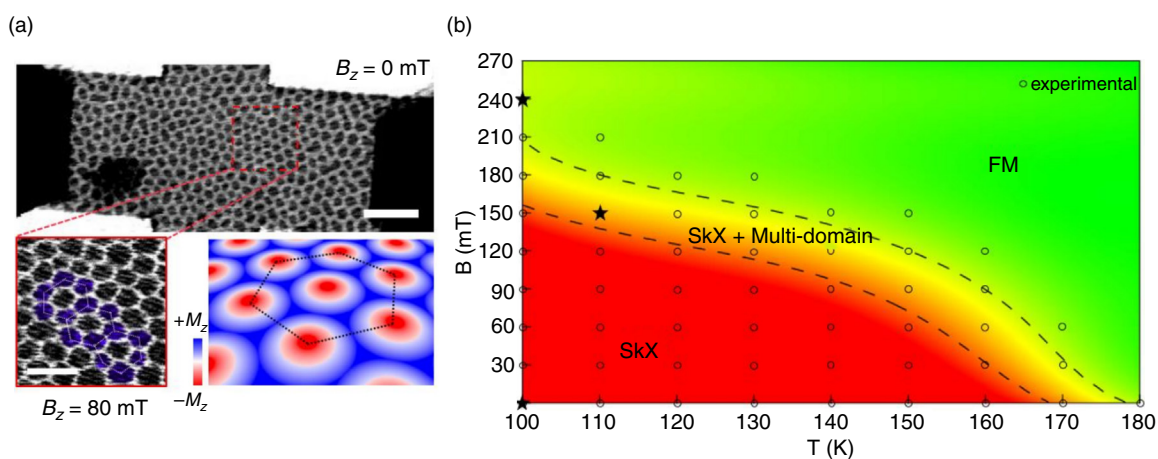

FIG. 6. Magnetic skyrmion lattice (SkX) phase in FGT. (a) Representative STXM image of skyrmion lattice stabilized over the whole FGT at $B_z = 0$ mT and T = 100 K. Scale bar = 2 μm. (b) Experimental phase diagram of magnetic configurations as a function of temperature and magnetic field. From Park *et al.*, arXiv:1907.01425 (2019). Licensed under a Creative Commons Attribution (CC BY) license.[116]
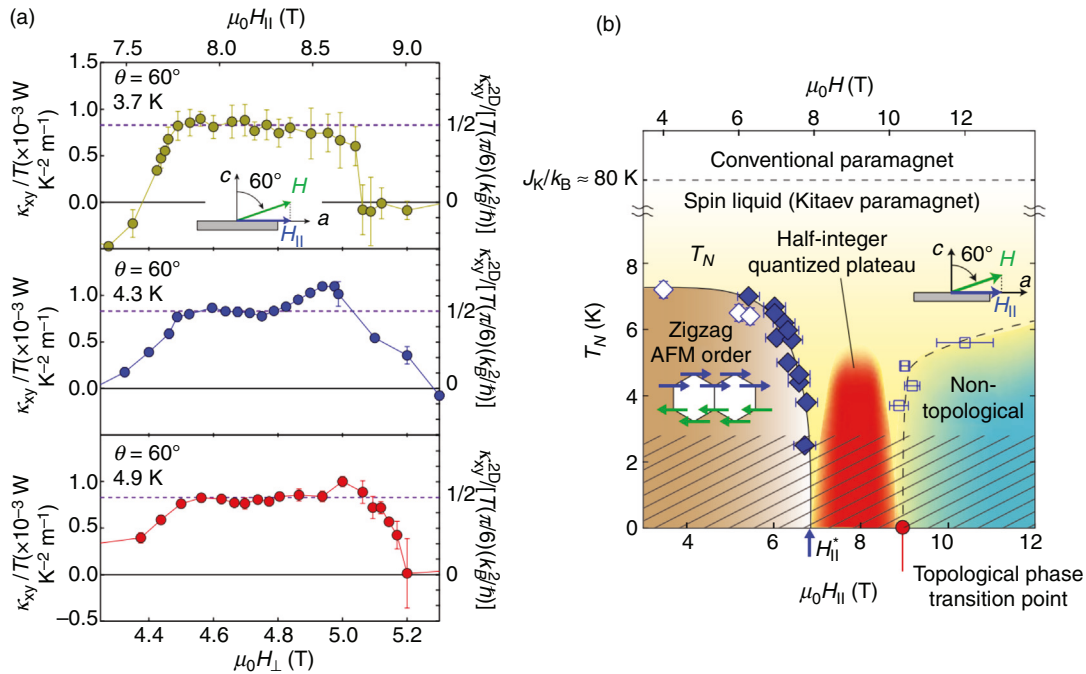
FIG. 7. Half-integer thermal quantum Hall effect in α-RuCl$_3$. (a) Here, we show the thermal Hall conductivity when applying tilted magnetic field on α-RuCl$_3$ at different temperatures; the half-integer plateau indicates the Majorana fermion, a signature of a Kitaev spin liquid phase. (b) Phase diagram of αRuCl$_3$ in a field tilted at $\theta = 60°$. Below T $\approx$ J$_K$/k$_B$ $\approx$ 80 K, the spin liquid (Kitaev paramagnetic) state appears. Reproduced with permission from Kasahara et al., Nature **559**(7713), 227–231 (2018). Copyright 2020 Macmillan Publishers Limited, part of Springer Nature.[120]

might energetically compete with each other to produce mixed-phase crystals.

In the very big picture, these crystal growth methods and isolation of mono- and few-layers of 2D magnets by exfoliation techniques present added complexities in translating these fundamental results from the laboratory setting to applications and, eventually, technology development. To this end, large-scale growth methods will be required in order to produce materials at wafer scales. This is a big ask for the materials synthesis community when the number of theoretically predicted 2D magnetic crystals is still increasing on a daily basis. As such, fast progress is needed to quickly identify the champion magnetic materials and develop more focused synthesis techniques to produce them at large scales (centimeter to 2-in. wafer). Here, the grand challenge will likely be in retaining their structural quality and defect profiles while increasing their lateral sizes. Nevertheless, general 2D growth techniques specific to halide-, phosphosulfide-, or chalcogen-based 2D vdW material systems will greatly benefit the 2D magnetism community in the long run by offering the foundations of 2D growth in these material systems.

Still, many questions emerge in the synthesis of atomically thin large-area 2D magnetic layers: Can large-area synthesis produce 2D sheets with environmental stability properties comparable to those in bulk crystals? Can we eliminate large defect densities like those observed in large-area 2D transition metal dichalcogenide systems? Can we engineer defects, strain, or pressure in these 2D magnets during synthesis by using a different choice of substrate, growth cooling profiles, or introduced defects? Can these sheets be synthesized on arbitrary substrates? Can we alloy 2D magnetic materials to unleash exciting opportunities similar to those realized in traditional materials alloying? These and many other overwhelming, but equally exciting questions are awaiting the materials synthesis community, and only brilliant work by researchers in the field will be capable of providing solid answers.

DATA AVAILABILITY STATEMENT

Data sharing is not applicable to this article as no new data were created or analyzed in this study.

REFERENCES

1. X. Wang, K. Du, Y. Y. Fredrik Liu, P. Hu, J. Zhang, Q. Zhang, M. H. S. Owen, X. Lu, C. K. Gan, P. Sengupta, C. Kloc, and Q. Xiong, 2D Mater. **3**(3), 031009 (2016).

2. J. U. Lee, S. Lee, J. H. Ryoo, S. Kang, T. Y. Kim, P. Kim, C. H. Park, J. G. Park, and H. Cheong, Nano Lett. **16**(12), 7433–7438 (2016).

3. B. Huang, G. Clark, E. Navarro-Moratalla, D. R. Klein, R. Cheng, K. L. Seyler, D. Zhong, E. Schmidgall, M. A. McGuire, D. H. Cobden, W. Yao, D. Xiao, P. Jarillo-Herrero, and X. Xu, Nature **546**(7657), 270–273 (2017).

4. C. Gong, L. Li, Z. Li, H. Ji, A. Stern, Y. Xia, T. Cao, W. Bao, C. Wang, Y. Wang, Z. Q. Qiu, R. J. Cava, S. G. Louie, J. Xia, and X. Zhang, Nature **546**(7657), 265–269 (2017).

5. M. Gibertini, M. Koperski, A. F. Morpurgo, and K. S. Novoselov, Nat. Nanotechnol. **14**(5), 408–419 (2019).

6. C. Gong and X. Zhang, Science **363**(6428), eaav4450 (2019).

7. K. S. Burch, D. Mandrus, and J. G. Park, Nature **563**(7729), 47–52 (2018).

8. N. D. Mermin and H. Wagner, Phys. Rev. Lett. **17**(22), 1133 (1966).

9. M. Alghamdi, M. Lohmann, J. Li, P. R. Jothi, Q. Shao, M. Aldosary, T. Su, B. P. T. Fokwa, and J. Shi, Nano Lett. **19**(7), 4400–4405 (2019).

10. Z. Wang, I. Gutiérrez-Lezama, N. Ubrig, M. Kroner, M. Gibertini, T. Taniguchi, K. Watanabe, A. Imamoğlu, E. Giannini, and A. F. Morpurgo, Nat. Commun. **9**(1), 2516 (2018).

11. D. Zhong, K. L. Seyler, X. Linpeng, R. Cheng, N. Sivadas, B. Huang, E. Schmidgall, T. Taniguchi, K. Watanabe, M. A. McGuire, W. Yao, D. Xiao, K. C. Fu, and X. Xu, Sci. Adv. **3**(5), e1603113 (2017).

12. D. Soriano, C. Cardoso, and J. Fernández-Rossier, Solid State Commun. **299**, 113662 (2019).

13. N. Sivadas, S. Okamoto, X. Xu, C. J. Fennie, and D. Xiao, Nano Lett. **18**(12), 7658–7664 (2018).

14. L. Thiel, Z. Wang, M. A. Tschudin, D. Rohner, I. Gutiérrez-Lezama, N. Ubrig, M. Gibertini, E. Giannini, A. F. Morpurgo, and P. Maletinsky, Science **364**(6444), 973–976 (2019).

15. N. Ubrig, Z. Wang, J. Teyssier, T. Taniguchi, K. Watanabe, E. Giannini, A. F. Morpurgo, and M. Gibertini, 2D Mater. **7**(1), 015007 (2019).

16. D. R. Klein, D. MacNeill, Q. Song, D. T. Larson, S. Fang, M. Xu, R. A. Ribeiro, P. C. Canfield, E. Kaxiras, R. Comin, and P. Jarillo-Herrero, Nat. Phys. **15**(12), 1255–1260 (2019).

17. Z. Wang, M. Gibertini, D. Dumcenco, T. Taniguchi, K. Watanabe, E. Giannini, and A. F. Morpurgo, Nat. Nanotechnol. **14**(12), 1116–1122 (2019).

18. A. Bedoya-Pinto, J.-R. Ji, A. Pandeya, P. Gargiani, M. Valvidares, P. Sessi, F. Radu, K. Chang, and S. Parkin, arXiv:2006.07605 (2020).

19. G. Menichetti, M. Calandra, and M. Polini, 2D Mater. **6**(4), 045042 (2019).

20. Y. Deng, Y. Yu, Y. Song, J. Zhang, N. Z. Wang, Z. Sun, Y. Yi, Y. Z. Wu, S. Wu, J. Zhu, J. Wang, X. H. Chen, and Y. Zhang, Nature **563**, 94–99 (2018).

21. Z. Fei, B. Huang, P. Malinowski, W. Wang, T. Song, J. Sanchez, W. Yao, D. Xiao, X. Zhu, A. F. May, W. Wu, D. H. Cobden, J.-H. Chu, and X. Xu, Nat. Mater. **17**(9), 778–782 (2018).

22. M. Bonilla, S. Kolekar, Y. Ma, H. C. Diaz, V. Kalappattil, R. Das, T. Eggers, H. R. Gutierrez, M.-H. Phan, and M. Batzill, Nat. Nanotechnol. **13**(4), 289–293 (2018).

23. J. Yang, W. Wang, Y. Liu, H. Du, W. Ning, G. Zheng, C. Jin, Y. Han, N. Wang, Z. Yang, M. Tian, and Y. Zhang, Appl. Phys. Lett. **105**(6), 063109 (2014).

24. J. Feng, D. Biswas, A. Rajan, M. D. Watson, F. Mazzola, O. J. Clark, K. Underwood, I. Markovic, M. McLaren, A. Hunter, D. M. Burn, L. B. Duffy, S. Barua, G. Balakrishnan, F. Bertran, P. L. Fevre, T. K. Kim, G. van der Laan, T. Hesjedal, P. Wahl, and D. C. King, Nano Lett. **18**(7), 4493–4499 (2018).

25. P. Chen, W. W. Pai, Y. H. Chan, V. Madhavan, M. Y. Chou, S. K. Mo, A. V. Fedorov, and T. C. Chiang, Phys. Rev. Lett. **121**(19), 196402 (2018).

26. A. O. Fumega, M. Gobbi, P. Dreher, W. Wan, C. Gonzalez-Orellana, M. Peña-Diaz, C. Rogero, J. Herrero-Martín, P. Gargiani, M. Ilyn, M. M. Ugeda, V. Pardo, and S. Blanco-Canosa, J. Phys. Chem. C **123**(45), 27802–27810 (2019).

27. D. J. O'Hara, T. Zhu, A. H. Trout, A. S. Ahmed, Y. K. Luo, C. H. Lee, M. R. Brenner, S. Rajan, J. A. Gupta, D. W. McComb, and R. K. Kawakami, Nano Lett. **18**(5), 3125–3131 (2018).

28. N. Mounet, M. Gibertini, P. Schwaller, D. Campi, A. Merkys, A. Marrazzo, T. Sohier, I. E. Castelli, A. Cepellotti, G. Pizzi, and N. Marzari, Nat. Nanotechnol. **13**(3), 246–252 (2018).

29. K. S. Novoselov, A. K. Geim, S. V. Morozov, D. Jiang, Y. Zhang, S. V. Dubonos, I. V. Grigorieva, and A. A. Firsov, Science **306**(5696), 666–669 (2004).

30. K. Kim, S. Y. Lim, J. Kim, J.-U. Lee, S. Lee, P. Kim, K. Park, S. Son, C.-H. Park, J.-G. Park, and H. Cheong, 2D Mater. **6**(4), 041001 (2019).

31. G. D. Nguyen, J. Lee, T. Berlijn, Q. Zou, S. M. Hus, J. Park, Z. Gai, C. Lee, and A.-P. Li, Phys. Rev. B **97**(1), 014425 (2018).

32. K. Nikonov, M. Brekhovskikh, A. Egorysheva, T. Menshchikova, and V. Fedorov, Inorg. Mater. **53**(11), 1126–1130 (2017).

33. M. Binnewies, R. Glaum, M. Schmidt, and P. Schmidt, *Chemical Vapor Transport Reactions* (Walter de Gruyter, 2012).

34. M. Binnewies, M. Schmidt, and P. Schmidt, Z. anorganische und allgemeine Chem. **643**(21), 1295–1311 (2017).

35. Y. Liu and C. Petrovic, Phys. Rev. B **97**(1), 014420 (2018).

36. M. Abramchuk, S. Jaszewski, K. R. Metz, G. B. Osterhoudt, Y. Wang, K. S. Burch, and F. Tafti, Adv. Mater. **30**(25), 1801325 (2018).

37. B. Kuhlow, Phys. Status Solidi (A) **72**(1), 161–168 (1982).

38. V. Atuchin, T. Gavrilova, T. Grigorieva, N. Kuratieva, K. Okotrub, N. Pervukhina, and N. Surovtsev, J. Cryst. Growth **318**(1), 987–990 (2011).

39. M. A. McGuire, G. Clark, K. Santosh, W. M. Chance, G. E. Jellison, Jr, V. R. Cooper, X. Xu, and B. C. Sales, Phys. Rev. Mater. **1**(1), 014001 (2017).

40. G. Lin, H. Zhuang, X. Luo, B. Liu, F. Chen, J. Yan, Y. Sun, J. Zhou, W. Lu, P. Tong, Z. G. Sheng, Z. Qu, W. H. Song, X. B. Zhu, and Y. P. Sun, Phys. Rev. B **95**(24), 245212 (2017).

41. X. Zhang, Y. Zhao, Q. Song, S. Jia, J. Shi, and W. Han, Jpn. J. Appl. Phys. **55**(3), 033001 (2016).

42. A. F. May, S. Calder, C. Cantoni, H. Cao, and M. A. McGuire, Phys. Rev. B **93**(1), 014411 (2016).

43. Z. Fisk and J. Remeika, Handbook Phys. Chem. Rare Earths **12**, 53–70 (1989).

44. O. Lopez-Sanchez, D. Lembke, M. Kayci, A. Radenovic, and A. Kis, Nat. Nanotechnol. **8**(7), 497–501 (2013).

45. H. Li, J. Wu, Z. Yin, and H. Zhang, Acc. Chem. Res. **47**(4), 1067–1075 (2014).

46. H. Li, G. Lu, Y. Wang, Z. Yin, C. Cong, Q. He, L. Wang, F. Ding, T. Yu, and H. Zhang, Small **9**(11), 1974–1981 (2013).

47. M. Grönke, P. Schmidt, M. Valldor, S. Oswald, A. Lubk, B. Büchner, and S. Hampel, Nanoscale **10**(40), 19014–19022 (2018).

48. M. Grönke, B. Buschbeck, P. Schmidt, M. Valldor, S. Oswald, Q. Hao, A. Lubk, D. Wolf, U. Steiner, and B. Büchner, Adv. Mater. Interfaces **6**(24), 1901410 (2019).

49. M. Grönke, D. Pohflepp, P. Schmidt, M. Valldor, S. Oswald, D. Wolf, Q. Hao, U. Steiner, B. Büchner, and S. Hampel, Nano-Struct. Nano-Objects **19**, 100324 (2019).

50. M. C. Wang, C. C. Huang, C. H. Cheung, C. Y. Chen, S. G. Tan, T. W. Huang, Y. Zhao, Y. Zhao, G. Wu, and Y. P. Feng, Annalen der Phys. **532**(5), 1900452 (2020).

51. S. Liu, X. Yuan, Y. Zou, Y. Sheng, C. Huang, E. Zhang, J. Ling, Y. Liu, W. Wang, C. Zhang, J. Zou, K. Wang, and F. Xiu, NPJ 2D Mater. Appl. **1**(1), 1–7 (2017).

52. W. Chen, Z. Sun, Z. Wang, L. Gu, X. Xu, S. Wu, and C. Gao, Science **366**(6468), 983–987 (2019).

53. P. Li, C. Wang, J. Zhang, S. Chen, D. Guo, W. Ji, and D. Zhong, Sci. Bull. **65**(13), 1064–1071 (2020).

54. H. Jiang, P. Zhang, X. Wang, and Y. Gong, Nano Res. **2020**, 1–13.

55. T. Gao, Q. Zhang, L. Li, X. Zhou, L. Li, H. Li, and T. Zhai, Adv. Opt. Mater. **6**(14), 1800058 (2018).

56. F. Reale, K. Sharda, and C. Mattevi, Appl. Mater. Today **3**, 11–22 (2016).

57. Z. Cheng, M. G. Sendeku, and Q. Liu, Nanotechnol. **31**(13), 135405 (2020).

58. T. A. Shifa, F. Wang, Z. Cheng, P. He, Y. Liu, C. Jiang, Z. Wang, and J. He, Adv. Funct. Mater. **28**(18), 1800548 (2018).

59. X. Sun, S. Zhao, A. Bachmatiuk, M. H. Rümmeli, S. Gorantla, M. Zeng, and L. Fu, Small **16**(29), 2001484 (2020).

60. H. Liu, X. Wang, J. Wu, Y. Chen, J. Wan, R. Wen, J. Yang, Y. Liu, Z. Song, and L. Xie, ACS Nano **14**(8), 10544–10551 (2020).

61. J. T. Ye, Y. J. Zhang, R. Akashi, M. S. Bahramy, R. Arita, and Y. Iwasa, Science **338**(6111), 1193–1196 (2012).

[62]Y. Cao, V. Fatemi, S. Fang, K. Watanabe, T. Taniguchi, E. Kaxiras, and P. Jarillo-Herrero, Nature **556**(7699), 43–50 (2018).

[63]Y. Wang, J. Xiao, H. Zhu, Y. Li, Y. Alsaid, K. Y. Fong, Y. Zhou, S. Wang, W. Shi, Y. Wang, A. Zettl, E. J. Reed, and X. Zhang, Nature **550**(7677), 487–491 (2017).

[64]S. Jiang, L. Li, Z. Wang, K. F. Mak, and J. Shan, Nat. Nanotechnol. **13**(7), 549–553 (2018).

[65]B. Huang, G. Clark, D. R. Klein, D. MacNeill, E. Navarro-Moratalla, K. L. Seyler, N. Wilson, M. A. McGuire, D. H. Cobden, D. Xiao, W. Yao, P. Jarillo-Herrero, and X. Xu, Nat. Nanotechnol. **13**(7), 544–548 (2018).

[66]H.-K. Mao, B. Chen, J. Chen, K. Li, J.-F. Lin, W. Yang, and H. Zheng, Matter Radiat. at Extremes **1**(1), 59–75 (2016).

[67]T. Li, S. Jiang, N. Sivadas, Z. Wang, Y. Xu, D. Weber, J. E. Goldberger, K. Watanabe, T. Taniguchi, C. J. Fennie, K. F. Mak, and J. Shan, Nat. Mater. **18**(12), 1303–1308 (2019).

[68]T. Song, Z. Fei, M. Yankowitz, Z. Lin, Q. Jiang, K. Hwangbo, Q. Zhang, B. Sun, T. Taniguchi, K. Watanabe, M. A. McGuire, D. Graf, T. Cao, J. H. Chu, D. H. Cobden, C. R. Dean, D. Xiao, and X. Xu, Nat. Mater. **18**(12), 1298–1302 (2019).

[69]H. J. Conley, B. Wang, J. I. Ziegler, R. F. Haglund, S. T. Pantelides, and K. I. Bolotin, Nano Lett. **13**(8), 3626–3630 (2013).

[70]W. Qing-Yan, L. Zhi, Z. Wen-Hao, Z. Zuo-Cheng, Z. Jin-Song, L. Wei, D. Hao, O. Yun-Bo, D. Peng, C. Kai, W. Jing, S. Can-Li, H. Ke, J. Jin-Feng, J. Shuai-Hua, W. Ya-Yu, W. Li-Li, C. Xi, M. Xu-Cun, and X. Qi-Kun, Chin. Phys. Lett. **29**(3), 037402 (2012) available at https://iopscience.iop.org/article/10.1088/0256-307X/29/3/037402/meta?casa_token=9Kx6eeyatrEAAAAA:ZQb9HP2GbgNGAmU7SNZRvuUM5809NjfQomktpmznKqNW_qhX-0qxSeEQ5hpTEn4vwUwP9T1lnLglfQE.

[71]S. S. Hong, M. Gu, M. Verma, V. Harbola, B. Y. Wang, D. Lu, A. Vailionis, Y. Hikita, R. Pentcheva, J. M. Rondinelli, and H. Y. Hwang, Science **368**(6486), 71–76 (2020).

[72]K. Cao, S. Feng, Y. Han, L. Gao, T. Hue Ly, Z. Xu, and Y. Lu, Nat. Commun. **11**(1), 284 (2020).

[73]L. Webster and J.-A. Yan, Phys. Rev. B **98**(14), 144411 (2018).

[74]F. Zheng, J. Zhao, Z. Liu, M. Li, M. Zhou, S. Zhang, and P. Zhang, Nanoscale **10**(29), 14298–14303 (2018).

[75]S. Jiang, H. Xie, J. Shan, and K. F. Mak, Nat. Mater. **19**, 1295–1299 (2020).

[76]P. C. Hohenberg, Phys. Rev. **158**(2), 383 (1967).

[77]J. G. Rau, E. K. Lee, and H. Y. Kee, Phys. Rev. Lett. **112**(7), 077204 (2014).

[78]T. Iwashita and N. Uryû, Phys. Rev. B **14**(7), 3090 (1976).

[79]I. Dzyaloshinsky, J. Phys. Chem. Solids **4**(4), 241–255 (1958).

[80]J. L. Lado and J. Fernández-Rossier, 2D Mater. **4**(3), 035002 (2017).

[81]D. Torelli, K. S. Thygesen, and T. Olsen, 2D Mater. **6**(4), 045018 (2019).

[82]S. M. Winter, A. A. Tsirlin, M. Daghofer, J. van den Brink, Y. Singh, P. Gegenwart, and R. Valenti, J. Phys. Condens. Matter **29**(49), 493002 (2017).

[83]N. Janša, A. Zorko, M. Gomilšek, M. Pregelj, K. W. Krämer, D. Biner, A. Biffin, C. Rüegg, and M. Klanjšek, Nat. Phys. **14**(8), 786–790 (2018).

[84]D. Pappas, K.-P. Kämper, and H. Hopster, Phys. Rev. Lett. **64**(26), 3179 (1990).

[85]J. B. Goodenough, *Magnetism and the Chemical Bond* (Interscience Publishers, 1963).

[86]A. S. Botana and M. R. Norman, Phys. Rev. Mater. **3**(4), 044001 (2019).

[87]M. A. McGuire, Crystals **7**(5), 121 (2017).

[88]S. Manzeli, D. Ovchinnikov, D. Pasquier, O. V. Yazyev, and A. Kis, Nat. Rev. Mater. **2**(8), 17033 (2017).

[89]V. Carteaux, D. Brunet, G. Ouvrard, and G. Andre, J. Phys. Condens. Matter **7**(1), 69 (1995).

[90]B. L. Chittari, Y. Park, D. Lee, M. Han, A. H. MacDonald, E. Hwang, and J. Jung, Phys. Rev. B **94**(18), 184428 (2016).

[91]W. Klingen, G. Eulenberger, and H. Hahn, Naturwissenschaften **57**(2), 88–88 (1970).

[92]S. Ogawa, J. Phys. Soc. Jpn. **15**(10), 1901–1901 (1960).

[93]Z. Xu and H. Zhu, J. Phys. Chem. C **122**(26), 14918–14927 (2018).

[94]R. D. Johnson, S. Williams, A. Haghighirad, J. Singleton, V. Zapf, P. Manuel, I. Mazin, Y. Li, H. O. Jeschke, and R. Valentí, Phys. Rev. B **92**(23), 235119 (2015).

[95]P. Reinhardt, M. Habas, R. Dovesi, I. de P. R. Moreira, and F. Illas, Phys. Rev. B **59**(2), 1016 (1999).

[96]S. Tian, J.-F. Zhang, C. Li, T. Ying, S. Li, X. Zhang, K. Liu, and H. Lei, J. Am. Chem. Soc. **141**(13), 5326–5333 (2019).

[97]K. Yang, F. Fan, H. Wang, D. Khomskii, and H. Wu, Phys. Rev. B **101**(10), 100402 (2020).

[98]T. Kong, K. Stolze, E. I. Timmons, J. Tao, D. Ni, S. Guo, Z. Yang, R. Prozorov, and R. J. Cava, Adv. Mater. **31**(17), 1808074 (2019).

[99]H. Wang, V. Eyert, and U. Schwingenschlogl, J. Phys. Condens. Matter **23**(11), 116003 (2011).

[100]K. Hirakawa, H. Kadowaki, and K. Ubukoshi, J. Phys. Soc. Jpn. **52**(5), 1814–1824 (1983).

[101]J. Cable, M. Wilkinson, E. Wollan, and W. Koehler, Phys. Rev. **127**(3), 714 (1962).

[102]M. Wilkinson, J. Cable, E. Wollan, and W. Koehler, Phys. Rev. **113**(2), 497 (1959).

[103]J. T. Heron, M. Trassin, K. Ashraf, M. Gajek, Q. He, S. Y. Yang, D. E. Nikonov, Y. H. Chu, S. Salahuddin, and R. Ramesh, Phys. Rev. Lett. **107**(21), 217202 (2011).

[104]S. M. Wu, S. A. Cybart, P. Yu, M. D. Rossell, J. X. Zhang, R. Ramesh, and R. C. Dynes, Nat. Mater. **9**(9), 756–761 (2010).

[105]C. Gong, E. M. Kim, Y. Wang, G. Lee, and X. Zhang, Nat. Commun. **10**(1), 2657 (2019).

[106]L. Zhao, T. L. Hung, C. C. Li, Y. Y. Chen, M. K. Wu, R. K. Kremer, M. G. Banks, A. Simon, M. H. Whangbo, C. Lee, J. S. Kim, I. Kim, and H. K. Kim, Adv. Mater. **24**(18), 2469–2473 (2012).

[107]L. Zhao, C.-C. Li, C.-C. Yang, and M.-K. Wu, arXiv:1911.11453 (2019).

[108]H. Tan, M. Li, H. Liu, Z. Liu, Y. Li, and W. Duan, Phys. Rev. B **99**(19), 195434 (2019).

[109]Q. Tong, F. Liu, J. Xiao, and W. Yao, Nano Lett. **18**(11), 7194–7199 (2018).

[110]M. Akram and O. Erten, arXiv:2008.01294 (2020).

[111]J. Liang, W. Wang, H. Du, A. Hallal, K. Garcia, M. Chshiev, A. Fert, and H. Yang, Phys. Rev. B **101**(18), 184401 (2020).

[112]A. K. Behera, S. Chowdhury, and S. R. Das, Appl. Phys. Lett. **114**(23), 232402 (2019).

[113]C. Xu, J. Feng, S. Prokhorenko, Y. Nahas, H. Xiang, and L. Bellaiche, Phys. Rev. B **101**(6), 060404 (2020).

[114]J. Yuan, Y. Yang, Y. Cai, Y. Wu, Y. Chen, X. Yan, and L. Shen, Phys. Rev. B **101**(9), 094420 (2020).

[115]D. Dey and A. S. Botana, Phys. Rev. Mater. **4**(7), 074002 (2020).

[116]T.-E. Park, L. Peng, J. Liang, A. Hallal, F. S. Yasin, X. Zhang, S. J. Kim, K. M. Song, K. Kim, M. Weigand, G. Schuetz, S. Finizio, J. Raabe, K. Garcia, J. Xia, Y. Zhou, M. Ezawa, X. Liu, J. Chang, H. C. Koo, Y. D. Kim, M. Chshiev, A. Fert, H. Yang, X. Yu, and S. Woo, Phys. Rev. B **103**, 104410 (2021).

[117]C. Broholm, R. J. Cava, S. A. Kivelson, D. G. Nocera, M. R. Norman, and T. Senthil, Science **367**(6475), eaay0668 (2020).

[118]S. H. Baek, S. H. Do, K. Y. Choi, Y. S. Kwon, A. U. B. Wolter, S. Nishimoto, J. van den Brink, and B. Buchner, Phys. Rev. Lett. **119**(3), 037201 (2017).

[119]S.-H. Do, S.-Y. Park, J. Yoshitake, J. Nasu, Y. Motome, Y. S. Kwon, D. Adroja, D. Voneshen, K. Kim, T.-H. Jang, J.-H. Park, K.-Y. Choi, and S. Ji, Nat. Phys. **13**(11), 1079–1084 (2017).

[120]Y. Kasahara, T. Ohnishi, Y. Mizukami, O. Tanaka, S. Ma, K. Sugii, N. Kurita, H. Tanaka, J. Nasu, Y. Motome, T. Shibauchi, and Y. Matsuda, Nature **559**(7713), 227–231 (2018).

[121]A. Banerjee, J. Yan, J. Knolle, C. A. Bridges, M. B. Stone, M. D. Lumsden, D. G. Mandrus, D. A. Tennant, R. Moessner, and S. E. Nagler, Science **356**(6342), 1055–1059 (2017).

[122]A. Banerjee, P. Lampen-Kelley, J. Knolle, C. Balz, A. A. Aczel, B. Winn, Y. Liu, D. Pajerowski, J. Yan, C. A. Bridges, A. T. Savici, B. C. Chakoumakos, M. D. Lumsden, D. A. Tennant, R. Moessner, D. G. Mandrus, and S. E. Nagler, NPJ Quantum Mater. **3**(1), 8 (2018).

[123]B. R. Ortiz, L. C. Gomes, J. R. Morey, M. Winiarski, M. Bordelon, J. S. Mangum, I. W. H. Oswald, J. A. Rodriguez-Rivera, J. R. Neilson, S. D. Wilson, E. Ertekin, T. M. McQueen, and E. S. Toberer, Phys. Rev. Mater. **3**(9), 094407 (2019).

[124]M. A. McGuire, Q. Zheng, J. Yan, and B. C. Sales, Phys. Rev. B **99**(21), 214402 (2019).